

TECHNOLOGY DEVELOPMENT FOR EXOPLANET MISSIONS

Technology Milestone Whitepaper

JPL Document D-81164

INTEGRATED CORONAGRAPH DESIGN AND WAVEFRONT AMPLITUDE CONTROL USING TWO DEFORMABLE MIRRORS

PROF. N. JEREMY KASDIN
PRINCIPAL INVESTIGATOR
PRINCETON UNIVERSITY
MECHANICAL AND AEROSPACE ENGINEERING

October, 2013

Coinvestigators and Collaborators:

Stuart Shaklan, Robert Vanderbei, Tyler D. Groff, Alexis Carlotti, Laurent Pueyo, Michael Carr,
A. J. Eldorado Riggs

Approvals

Released by:



10/15/2013

N. Jeremy Kasdin
Principal Investigator, Princeton University

Approved by:



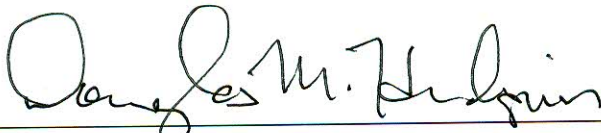
10/29/2013

Peter R. Lawson
Exoplanet Exploration Program Chief Technologist, JPL



10/29/2013

Gary Blackwood
Exoplanet Exploration Program Manager, JPL



11/13/13

Douglas Hudgins
Exoplanet Exploration Program Scientist, NASA HQ



11/13/13

Anthony Carro
Exoplanet Exploration Program Executive, NASA HQ

CONTENTS

1. Objectives	4
2. Coronagraphy and Amplitude Control	5
2.1. How coronagraphs achieve high contrast	5
2.2. Broadband wavefront control with 2 DMs	7
2.3. Focal Plane Wavefront Estimation	8
2.4. Wavefront Correction of Broadband Amplitude and Phase Errors	9
3. Milestone and Experiment Description	12
3.1. Milestone description	12
3.2. Test Preparation and Modifications at the HCIT	12
3.3. Mask design and manufacture	13
3.4. Experiment Risks	15
4. Contrast Measurement and Data Analysis	17
4.1. Definitions	17
4.2. Measurement of the Star Brightness	18
4.3. Measurement of the Coronagraph Contrast Field	18
4.4. Milestone Demonstration Procedure	19
4.5. Milestone Contrast Measurement and Confidence Limit	19
5. Success criteria	23
6. Certification & Data sharing	24
7. List of Acronyms	25

1. OBJECTIVES

A coronagraph for achieving high contrast is one of the two key technologies being studied for exoplanet imaging (the other being an external starshade). While many different types of coronagraphs have been proposed, all operate in the same basic architecture: using masks, stops, and mirrors to modify the beam path and thus produce high contrast in the final image. More importantly, all require wavefront control systems to correct for amplitude and phase aberrations in the optical system in order to recover the high-contrast performance.

All coronagraphs work on the same principle—they modify the amplitude of the electric field across the exit pupil in order to create a final high-contrast image. This may be done through apodization, phase plates, remapping, or phase and amplitude adjustment at intermediate image planes. Nevertheless, in every case, high contrast can only be achieved through a change in the field’s amplitude. Unfortunately, phase and amplitude errors in the telescope limit the achievable contrast, often to no better than a contrast of 10^{-5} . All practical systems must then include the capability for both amplitude and phase control of the wavefront; even under the most rigorous manufacturing and assembly tolerances, various wavefront aberrations from the optical assembly produce bright speckles in the image plane that must be removed from the “discovery” region, creating a so-called “dark hole” where planets can be found. Current laboratory experiments using a single deformable mirror (DM) have employed wavefront estimation and correction algorithms that are capable of generating regions of better than 10^{-9} contrast in broadband ($\Delta\lambda/\lambda = 10\%$) light but on only one side of the image plane. [?] Achieving broadband control in dark holes on both sides of the image plane requires direct control over amplitude. [?]

? first suggested using two DMs in a Michelson configuration to correct amplitude. ? and ? showed that amplitude and phase correction can be accomplished using two deformable mirrors in series, leveraging the Talbot effect for field propagation (phase-to-amplitude conversion). In fact, ? showed that using a third DM can allow correction of higher-order errors and thus dark holes over broader bands of wavelengths.

All experiments to date at the High Contrast Imaging Testbed (HCIT) at JPL, however, have been done with a single deformable mirror; amplitude errors are corrected by creating a dark hole on only one side of the image plane. Nevertheless, instrument concepts being proposed or considered for future missions all include two deformable mirrors in series so that both amplitude and phase can be corrected. The Princeton High-Contrast Imaging Laboratory (HCIL) is currently the only facility with two deformable mirrors operating in series. We have successfully generated broadband dark holes on both sides of the central Point Spread Function (PSF) in the image plane of the system, though at only modest contrast.[???] We have operational algorithms that have been developed over the past several years as part of NASA Astronomy and Physics Research and Analysis (APRA) and NASA Engineering and Space Science Fellowship (NESSF) grants that have been proven experimentally in our laboratory environment (TRL 3). The limiting contrast in the HCIL is primarily driven by the fact that the facility is in air and not temperature controlled. This TDEM is intended to demonstrate the ability to create higher contrast on both sides of the image plane with a shaped pupil coronagraph using two sequential DMs at the HCIT.

For this TDEM the HCIT will be modified to incorporate two deformable mirrors in series with a shaped pupil. We will use a shaped pupil of similar design to that for our successful 2007 test (where we achieved roughly 10^{-9} contrast monochromatically and 2×10^{-9} contrast in a 10% band). Our primary objective is to demonstrate two dark holes on both sides of the image plane in monochromatic light by keeping as much as possible the same as our 2007 test but incorporating two DMs. If successful, our secondary goal is to attempt to create the same dark holes in a 10% band. We define our milestones for an average contrast over a dark hole. We treat this average contrast as a random variable over multiple experiments. We then define our milestones using a typical 3-sigma criterion:

TDEM Primary Milestone:

- Demonstrate with 90% confidence that the system can achieve symmetric dark holes in the image plane in monochromatic light with an expected average contrast plus 3-sigma $\leq 1 \times 10^{-9}$ from 5-9 λ/D using two deformable mirrors in series.

TDEM Secondary Milestone:

- Demonstrate with 90% confidence that the system can achieve symmetric dark holes in the image plane in a 10% band about the central wavelength with an expected average contrast plus 3-sigma $\leq 5 \times 10^{-9}$ from 5-9 λ/D using two deformable mirrors in series.

The detailed statistical analysis is given in § 4.5. Achieving the milestones in this TDEM will bring this critical amplitude control capability to TRL 4 and will demonstrate for the first time the effectiveness of the two-deformable-mirror approach to achieving amplitude control.

2. CORONAGRAPHY AND AMPLITUDE CONTROL

2.1. How coronagraphs achieve high contrast.

All coronagraphs produce an electric field at the imaging element with a different wavefront amplitude than that entering the system. A coronagraph that only modifies phase does not achieve the needed high-contrast at the desired inner working angle. As a result, in the presence of amplitude and phase errors, the ability to achieve high contrast is only as good as the ability to correct amplitude in the wavefront control system. To see this, we can develop a general expression for the contrast in any coronagraph. For simplicity, we treat the problem in one dimension; the generalization to two dimensions is straightforward.

Consider a simple imaging system with a uniform, on-axis entrance electric field which we normalize to unity and an aperture shape function given by $A_e(x)$. The point spread function of the telescope is then just the square of the Fourier transform of the entrance aperture,

$$(1) \quad P_0 = |F(\omega)|^2 = |\mathcal{F}\{A_e(x)\}|^2.$$

Next, suppose that a coronagraph is placed between the entrance field and the imaging element. The coronagraph is a linear system that changes the amplitude and phase of the electric field so that the field at the imaging element is given by

$$(2) \quad E_1 = \mathcal{C}\{A_e(x)\} = A_o(x)e^{i\phi(x)}$$

where $A_o(x)$ is the amplitude change due to the coronagraph and $\phi(x)$ is the phase change. The point spread function is now,

$$(3) \quad P_1 = |F_1(\omega)|^2 = |\mathcal{F}\{A_o(x)e^{i\phi(x)}\}|^2.$$

Let Ω be the inner working angle of the coronagraph and Δ_Ω be the are of the region of high-contrast bounded by Ω . The contrast can be defined as the ratio of the integrated intensity in the discovery space at the inner working angle, Δ_Ω , to the peak of the point spread function of the open aperture system,

$$(4) \quad C = \frac{\int_{\Delta_\Omega} |F_1(\omega)|^2 d\omega}{T_\Omega \Delta_\Omega |F(0)|^2}$$

where we have also normalized by the throughput of the coronagraph system at the inner working angle, T_Ω . Since we are assuming the system without the coronagraph is just an open aperture,

$F(0) = D$, the diameter of the telescope (it equals the area in the two-dimensional problem). We thus rewrite Eq. 4,

$$(5) \quad C = \frac{1}{2T_{\Omega}\Delta_{\Omega}D^2} \left[\int_{-\infty}^{\infty} |F_1|^2 d\omega - \int_{\Delta_C} |F_1|^2 d\omega \right]$$

where Δ_C is the complementary region of the image plane to the discovery space.

From Parseval's theorem,

$$(6) \quad \int_{-\infty}^{\infty} |F_1|^2 d\omega = \int_{-D/2}^{D/2} |A(x)|^2 dx$$

where, again, $A(x)$ is the amplitude distribution at the exit pupil. This lets us rewrite the contrast,

$$(7) \quad C = \frac{\int_{-D/2}^{D/2} |A(x)|^2 dx}{2T_{\Omega}\Delta_{\Omega}D^2} \left[1 - \frac{\int_{\Delta_C} |F_1|^2 d\omega}{\int_{-\infty}^{\infty} |F_1|^2 d\omega} \right].$$

Eq. 7 is the most general expression for the contrast created from an on-axis field passing through *any* coronagraph. It shows that coronagraphs achieve contrast in one of two ways. The first is to reduce the field amplitude at the exit of the coronagraph, making the leading factor (the integral of $|A(x)|^2$ in Eq. 7) sufficiently small. Examples of such coronagraphs include the Lyot, Bandlimited Lyot, Vector Vortex, Four Quadrant Phase Mask, Achromatic Interfering Coronagraph (AIC), and any other coronagraph that modifies an intermediate image to change the amplitude of the exit pupil field. In fact, the bandlimited Lyot coronagraph, for example, makes $A(x)$ identically zero, thus removing all starlight.

The second approach to creating contrast is to make the factor in brackets small. This is accomplished by making the ratio of integrated intensity outside the discovery space to the total integrated intensity as close to one as possible. In other words, by concentrating as much energy as possible outside the discovery space, high contrast can be achieved. All apodized coronagraphs operate this way, including smooth apodizers, shaped pupils, and pupil mapping coronagraphs (PIAA). The Apodized Pupil Lyot Coronagraph (APLC) creates high contrast through a combination of both terms. We note that for every imaging system, with or without a coronagraph, the discovery space Δ_{Ω} can be made sufficiently far away (large enough inner working angle) to achieve any desired contrast. However, to achieve contrast for a sufficiently small Ω in a reasonable size telescope, the amplitude of the field at the exit pupil must be changed. We know this from the finite uncertainty principle. [?] In fact, the optimal amplitude change (apodization) that creates the most contrast for a given inner working angle is the prolate spheroidal wave function; that is, it maximally concentrates energy outside of Δ_{Ω} . [?]

In order to create contrast, *every* coronagraph modifies the amplitude of the exit field. The ability to create a sufficiently dark discovery space is therefore limited by the amplitude errors in the optical system and the ability to correct them. For a wavefront control system that only corrects phase, the contrast will eventually be limited by amplitude errors (the amount $A(x)$ differs from the designed for value). To achieve the extremely high contrast necessary for terrestrial planet imaging, an amplitude control device is mandatory. The result here also implies that it may be unnecessary to design a coronagraph to achieve contrast any better than the level determined by the existing amplitude errors (including those in the coronagraph). It may be possible to use the amplitude control device to create the dark hole below the nominal level of the coronagraph, thus allowing smaller inner working angle or higher throughput (essentially, the two deformable mirrors are being used as pupil mappers). We have an ongoing effort to demonstrate this at Princeton and it is a tertiary goal of this TDEM. We are making a mask only designed to achieve 10^{-7} contrast in order to test this concept in the HCIT. However, it is not part of our milestones.

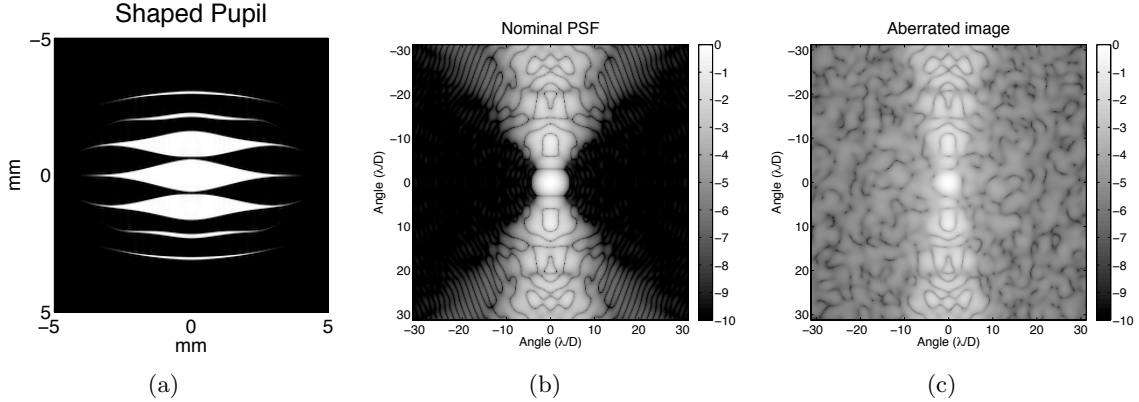


FIGURE 1. (a) A shaped pupil. (b) The ideal PSF of a system with the shaped pupil shown. (c) The image from the same system with simulated aberrations. The phase aberration was generated to have an amplitude of $\lambda/400$ with a $-3/2$ power law, and the amplitude aberration has an amplitude of $1/1000$ with a -2 power law. The aberration levels are similar to those measured in the Princeton HCIL. The units of the images are in λ/D and the scale is $\log(\text{contrast})$.

2.2. Broadband wavefront control with 2 DMs.

In the Princeton High Contrast Imaging Laboratory (HCIL) we have been studying wavefront sensing and control algorithms using a shaped pupil coronagraph. Shaped pupils have the advantage of being simple to design and manufacture without complicated optics and with no chromaticity. [?] Figure 1 illustrates a ripple shaped pupil being used in our lab, its diffraction properties using perfect optics, and its diffraction properties in the presence of aberrations. It is these speckles introduced by aberrations that limit the ability to image planets and necessitate the use of wavefront control. Figure 2 shows our results using a shaped pupil with wavefront control at the High Contrast Imaging Testbed at the Jet Propulsion Laboratory in 2007 where we created a dark hole with close to 10^{-9} contrast on one side of the image plane, the highest achieved contrast at that time. [?] This demonstrates the effectiveness of our algorithms, our process for manufacturing shaped pupils, and our proven ability to operate in the HCIT facility. Nevertheless, because only a single DM was used for correction, amplitude errors limit the dark hole to only a single side of the PSF. Correcting amplitude errors on both sides of the image requires two deformable mirrors, a capability not yet implemented at the HCIT.

Since 2007 we have been performing experiments at Princeton’s HCIL using two DMs in series for broadband control. A schematic of our current experimental layout is shown in Figure 3. [?] The algorithms we use can be divided into two components, an estimation algorithm and a correction algorithm. The estimation algorithm determines the wavefront at the image plane given a set of intensity measurements. The correction algorithm uses the estimate of the image plane electric field to determine the DM commands necessary to suppress aberrations in the search area, commonly referred to as a dark hole. Several wavefront estimation and control schemes have been developed and tested at Princeton’s HCIL [????]. Currently, we use the DM-diversity estimation scheme described below with a correction algorithm called “stroke minimization” [?]. This employs an optimization to minimize actuator voltages with a target contrast constraint. The ability of this correction algorithm to achieve the desired contrast in minimum time is limited both by the accuracy of the field estimates and the precision of the DM model used to relate the calculated DM shapes to actuator voltages.

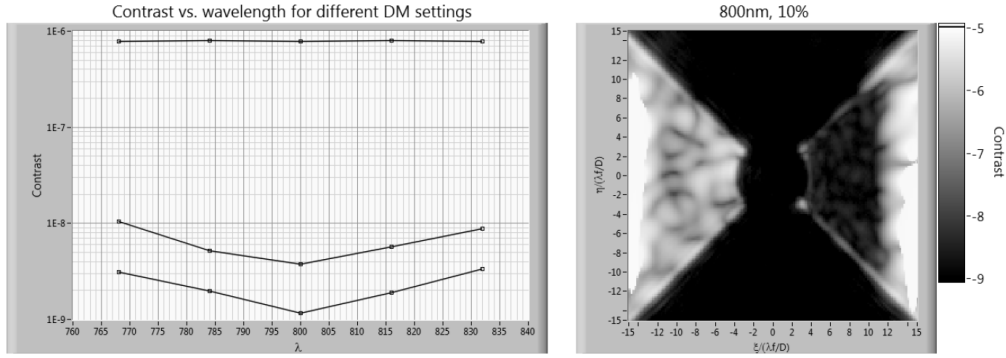


FIGURE 2. Contrast achieved at the HCIT in 2007 with a ripple shaped pupil and single DM. *Left:* Plots of contrast vs. wavelength for different DM settings. *Right:* Post-correction image in the full 10% band showing 2.4×10^{-9} contrast in the dark zone between 4 and $10 \lambda_0/D$.

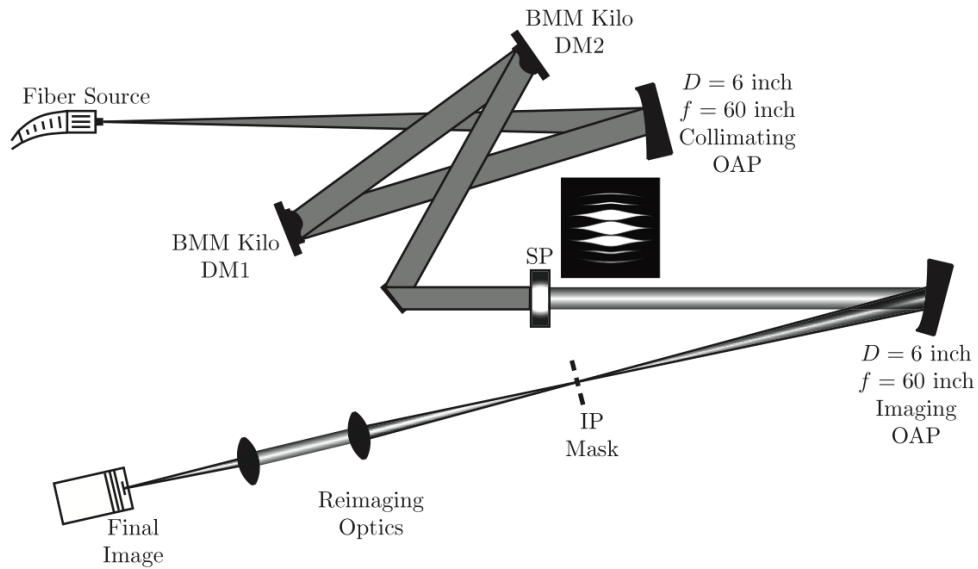


FIGURE 3. Current Princeton HCIL testbed layout.

2.3. Focal Plane Wavefront Estimation.

Focal plane wavefront sensing (FPWS) techniques rely on focal plane measurements to estimate the electric field aberrations. These estimates are coupled with wavefront correction techniques that apply voltage commands to a DM to improve the contrast in the focal plane. Due to nonlinearities in the system, all current algorithms iterate to achieve the desired final contrast.

Wavefront sensing outside the focal plane, which is common in ground-based AO applications, is limited by the non-common path errors between the wavefront sensor and the focal plane. [?] Princeton has been one of the leaders in the development of FPWS wavefront estimation and control techniques for high-contrast imaging in space. [??] Our most mature wavefront estimation technique employs a pairwise DM-diversity algorithm which applies known shapes on the DM to estimate the field using a focal plane detector.

DM diversity estimation of the electric field requires multiple images and is based on a pairwise estimation scheme devised by ? where multiple conjugate DM settings are introduced to form

known intensity patterns at the image plane so that their differences can be used to reconstruct the complex electric field. [?]

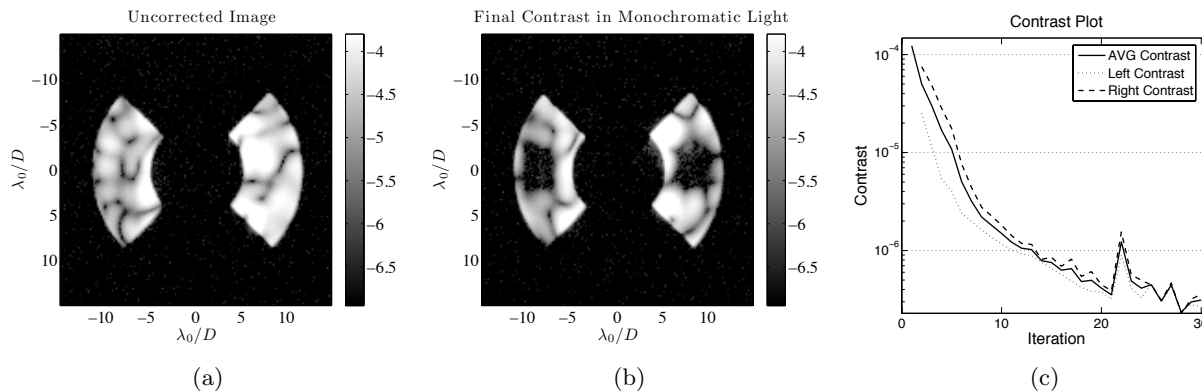


FIGURE 4. Experimental results of correction using two sequential DMs and the DM diversity wavefront estimation algorithm in $5 \times 6 \lambda/D$ regions. (a) The aberrated image. (b) The corrected image. (c) Contrast plot. Two-dimensional images are in units of $\log(\text{contrast})$.

Our best contrast results to date have been obtained using this estimation algorithm correcting over a region from $6\text{--}11 \lambda/D$ in the horizontal direction and -3 to $+3 \lambda/D$ in the vertical direction. By using two sequential DMs we were able to create dark holes with similar dimensions on either side of the image plane. [??]

Figure 4 shows recent HCIL experimental aberrated and corrected images as well as contrast plots across the dark hole regions in the image plane. The image plane mask is covering the PSF we expect to see from the simulations shown in Figure 1(c). The average contrast in the small dark holes is reduced by just under three orders of magnitude to 2.3×10^{-7} on both sides of the image plane.

In our most recent results, we have reproduced our best contrast level with a closed-loop, Kalman filter algorithm developed by ?. This estimator utilizes the same probe shapes as DM Diversity but requires just one new image pair each iteration to update the estimate of the image plane electric field. Fewer image pairs each iteration greatly reduces the time required to achieve high contrast, since exposures and not computations are the most time intensive part of the experiment. Our plan is to use the Kalman filter algorithm in our experiments at the HCIT.

2.4. Wavefront Correction of Broadband Amplitude and Phase Errors.

Narrowband correction schemes ($\Delta\lambda/\lambda \leq 2\%$) for high contrast imaging have been well demonstrated. [??] Nevertheless, achieving broadband correction is key to raising the TRL of wavefront control algorithms. Generating a null for each wavelength separately to spectrally characterize a target (as currently done in most laboratories) would be prohibitively slow because of the large number of exposures required to estimate the electric field. A broadband algorithm reduces the number of exposures, and hence the time required to spectrally characterize a target. Increasing the bandwidth is also the easiest way to increase the number of photons in an inherently photon limited system, reducing the exposure time required to achieve a planetary detection. Thus broadening the spectral range of the wavefront correction will improve the overall efficiency of a planet finding mission and will allow for fewer parallel beam paths, making it cheaper and less complex to measure over a broad bandwidth. ? showed that two DMs in series can be used to correct over a broader range of wavelengths by incorporating a wavelength expansion of the aberrated electric

field propagation. This was shown by expressing the aberrated field at a pupil, given in terms of the amplitude and phase aberrations, $r(x, y)$ and $\phi(x, y)$ respectively, as a Fourier series. The result is an expansion of the wavefront aberrations in powers of $1/\lambda$. ? showed that with 2 DMs it is possible to correct the $1/\lambda$ and λ independent terms in the expansion.

As mentioned earlier, our approach to finding DM settings is through a stroke minimization algorithm where we find the smallest stroke that will achieve a desired contrast constraint. Modifying this for broadband is done by simply augmenting the constraint for multiple wavelengths above and below the central wavelength. This optimization problem can be written as

$$\begin{aligned}
 (8) \quad & \text{minimize} && \sum_{k=1}^N a_k^2 = XX^T \\
 & \text{subject to:} && I_{DZ}(\lambda_0) \leq 10^{-C_{\lambda_0}}, \\
 & && I_{DZ}(\lambda_1) \leq 10^{-C_{\lambda_1}}, \\
 & && I_{DZ}(\lambda_2) \leq 10^{-C_{\lambda_2}} \\
 & \text{where} && \lambda_1 = \gamma_1 \lambda_0 \\
 & && \lambda_2 = \gamma_2 \lambda_0,
 \end{aligned}$$

which minimizes actuator strokes, X , under the constraint that a particular contrast be achieved, C_i , in three separate wavelengths, λ_i . The cost function to be minimized, J , then takes on the same basic form as the monochromatic case, but now includes multiple wavelengths in the Lagrange multipliers,

$$\begin{aligned}
 J = X & \left[\mathcal{I} + \mu \frac{4\pi^2}{\lambda_0^2} (M_{\lambda_0} + \delta_1 M_{\lambda_1} + \delta_2 M_{\lambda_2}) \right] X^T + \mu \frac{4\pi}{\lambda_0} [\mathfrak{S}\{b_{\lambda_0}\} + \delta_1 \mathfrak{S}\{b_{\lambda_1}\} + \delta_2 \mathfrak{S}\{b_{\lambda_2}\}] X^T \\
 & + \mu [(d_{\lambda_0} - 10^{-C_{\lambda_0}}) + \delta_1 (d_{\lambda_1} - 10^{-C_{\lambda_1}}) + \delta_2 (d_{\lambda_2} - 10^{-C_{\lambda_2}})]
 \end{aligned}$$

where M_λ describe the effect on the image plane intensity from the DM actuation, b_λ is intensity from the interaction of the DMs with the aberrated field, and d_λ is intensity of the uncorrected aberrated field. The multipliers δ_1 and δ_2 allow us to parameterize a single Lagrange multiplier in the cost function. In the more general case with three Lagrange multipliers it is possible that the global minimum of the function would not result in constant contrast at each wavelength. This approach to stroke minimization, what we call “windowed stroke minimization”, makes the optimization in wavelength tractable and allows for estimation only at a single wavelength, which reduces the number of exposures required for correction over a bandwidth defined by the upper and lower bounding wavelengths.

Providing estimates for this algorithm becomes more complicated because it requires field values at multiple wavelengths. Taking estimates for each wavelength is no better than correcting each wavelength individually because estimation is the most costly component of the control algorithm and the time required is limited by exposure time, not computation. We solved this by extrapolating a single monochromatic estimate to higher and lower wavelengths by approximating the pupil field expansion from ?. By assuming that amplitude distributions are wavelength independent and phase distributions scale as $1/\lambda$, we approximate the pupil plane electric field by

$$(9) \quad E_{pup}(u, v, \lambda) \approx A(u, v) e^{i2\pi \frac{\lambda_0}{\lambda} \phi_0(u, v)}.$$

Given a linear, wavelength dependent, transformation between the pupil and image plane \mathcal{C}_λ (eg. the optical Fourier transform) we can use Eq. 9 to describe the electric field estimate at an arbitrary wavelength λ as a function of the image plane electric field estimate taken at the original

wavelength λ_0 using the DM-diversity algorithm. With the wavelength dependence only appearing in the phase of the pupil field and in the pupil-to-image transformation the electric field estimate at a new wavelength becomes

$$(10) \quad E_{est}(x, y, \lambda) = C_\lambda \left\{ \frac{C_{\lambda_0}^{-1} \{E_{est}(\lambda_0)\}^{\frac{\lambda_0}{\lambda}}}{|C_{\lambda_0}^{-1} \{E_{est}(\lambda_0)\}|^{\frac{\lambda_0}{\lambda} - 1}} \right\}.$$

Figure 5 shows laboratory results at the HCIL creating symmetric dark holes in broadband using the windowed stroke minimization algorithm and extrapolated estimation from Eq. 10. [?] Currently the achievable contrast by extrapolating estimates is 4.91×10^{-6} over a $\sim 10\%$ band (Figure 5(a)-5(c)) and 1.48×10^{-5} over the full bandwidth (300-800 nm, Figure 5(f)).

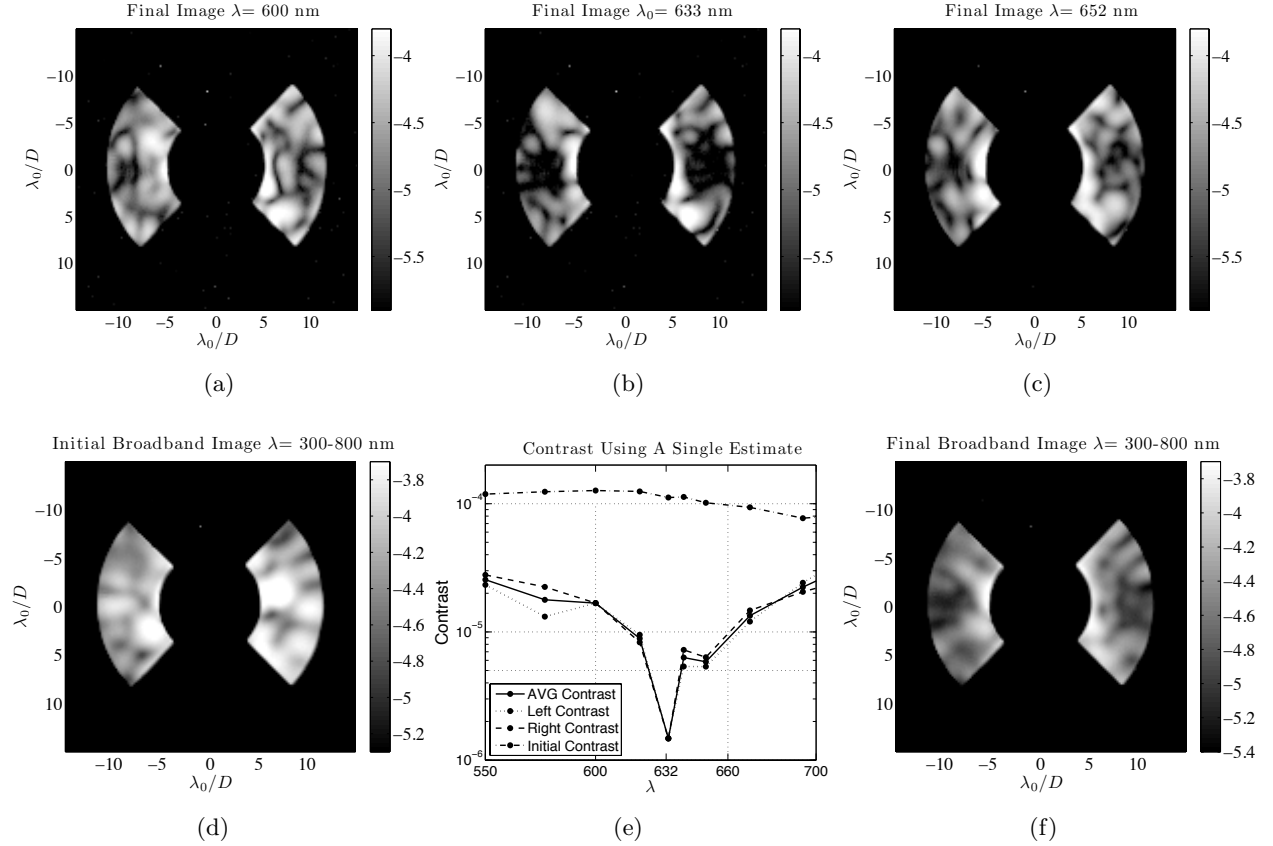


FIGURE 5. Single estimate with extrapolation technique to the bounding wavelengths. a) $\sim .95\lambda_0$ lower bounding wavelength. b) Estimated Wavelength. c) $\sim 1.05\lambda_0$ upper bound. d) Uncorrected broadband image. e) Contrast vs. Wavelength. f) Corrected Broadband Image (300 - 800 nm)

There are two related sources that limit our ability to create higher broadband contrast. The first is the quality of our DM model. Since both the estimation and control algorithms incorporate DM surface models and actuator voltage maps, errors in this mapping directly translate into limitations in contrast. The second source is the extent to which the aberrated field over the wavelength band is well represented by the first two terms in a wavelength expansion. Two DMs in series can only correct the λ independent and $1/\lambda$ terms. [?] Increasing the size of the $1/\lambda^2$ terms, as might happen with poor surface quality on the DMs, translates directly into contrast floors and

limited bandwidth. Both of these sources will be partially mitigated at Princeton’s HCIL by two new, higher quality deformable mirrors being supplied under a separate TDEM. By improving the surface quality of the DMs, the higher order terms become less important and the model becomes easier to predict. This will allow us to improve our contrast measurements at the HCIL (eventually being limited only by the ambient environment and power fluctuations in the lasers) and better prepare for tests at the HCIT. We also expect better performance at the HCIT because of the higher surface quality of the DMs there. Broadband limitations can also be mitigated by incorporating a third DM, either in series or in a Michelson arrangement. [?] Adding two new DMs to our laboratory opens the possibility of experimenting with three-DM designs and thus determining the limitations on bandwidth and contrast from the higher order terms in the wavefront expansion.

Both the control and estimation algorithms use several approximations to make them tractable. In the control, the main approximation is to linearize phase of the DM surfaces through the coronagraph to the image plane. It is this linearization that results in the need to iterate the control algorithm. The accuracy of the control can be improved somewhat by relinearizing at each step, but the commands are small enough to the DM that this hasn’t proven to be necessary. Likewise, the diversity estimation scheme uses a linearized expression to find the field estimate. The most significant approximation is the extrapolation used to estimate the field at multiple wavelengths. This is the primary limit of our current ability to do broadband control. All other broadband experiments at the HCIT uses multiple measurements at each wavelength. One of our goals is to explore how well we can perform broadband control using extrapolation.

3. MILESTONE AND EXPERIMENT DESCRIPTION

3.1. Milestone description. Because this is the first time that two deformable mirrors will be used in the HCIT, we are being modest in our objectives. As we will describe below, there are still a number of unknowns regarding the performance of the dual DMs. In particular, the configuration, for practical reasons, is unlike our lab or any potential instrument design. Our goal is thus to show that two DMs in series can be used to correct amplitude and thus create two symmetric dark holes of modest inner working angle in monochromatic light. If all goes well, we also hope to demonstrate broadband performance (over a 10% band about the central wavelength) with a result similar to that obtained in 2007 for a single-sided dark hole. Our primary and secondary milestones are thus:

TDEM Primary Milestone:

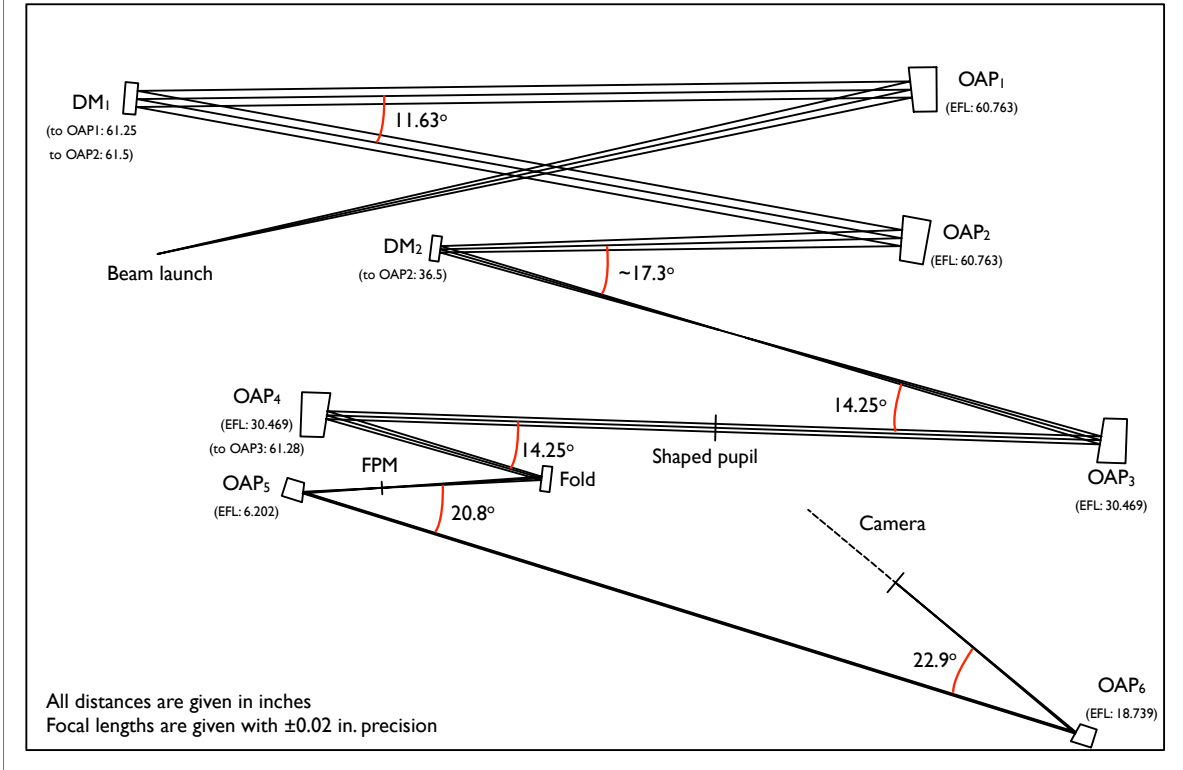
- Demonstrate with 90% confidence that the system can achieve symmetric dark holes in the image plane in monochromatic light with an expected average contrast plus 3-sigma $\leq 1 \times 10^{-9}$ from 5-9 λ/D using two deformable mirrors in series.

TDEM Secondary Milestone:

- Demonstrate with 90% confidence that the system can achieve symmetric dark holes in the image plane in a 10% band about the central wavelength with an expected average contrast plus 3-sigma $\leq 5 \times 10^{-9}$ from 5-9 λ/D using two deformable mirrors in series.

3.2. Test Preparation and Modifications at the HCIT. The main purpose of our experiments in the HCIT is to use two deformable mirrors (DM) in series, in non-conjugate planes, to create symmetric dark holes in the image plane. Since only a single DM has been used so far in the HCIT, the optical layout had to be revisited to accommodate a second DM. Because the HCIT needs to be returned to its original configuration for subsequent tests by other groups using only a single DM, JPL determined that the modifications made to the layout must have the smallest footprint possible, so that the second DM (DM_2) can be removed as soon as our tests are done. As a result,

HCIT Layout - adapted from B. Kern



Thursday, June 6, 13

FIGURE 6. Optical layout of the HCIT. DM_2 is located downstream of OAP_2 , and upstream of OAP_3 , in lieu of the fold mirror usually located there.

placing DM_2 in a collimated beam, a few feet after DM_1 , required too significant a change. It would have required OAP_2 to move and the rest of the optics or, alternatively, the beam launch, OAP_1 , and DM_1 . It was thus decided to replace the fold mirror located downstream of OAP_2 with DM_2 (see Fig.6). As a result, DM_2 is located in a converging beam instead of a collimated beam. This is a fundamental difference with the optical layout of the HCIL in Princeton, especially since the distance between OAP_2 and DM_2 equals $3/5$ of the effective focal length of OAP_2 .

The two-DM wavefront control in Princeton uses two 32 by 32 BMC DMs, and the second main difference between Princeton HCIL and the HCIT layout is that DM_1 and DM_2 do not have the same number of actuators, nor do the beams intercept the same number of actuators. In the HCIT, DM_1 has 64 actuators along each axis. Because of the surface flatness of the DM, only the inner 48 to 56 actuators are usually used (depending on choice of pupil stop). In the two-DM HCIT, the 56 actuators on DM_1 are remapped onto 22.4 actuators on DM_2 . As described above, one of the significant tasks for the test is to rewrite the control algorithms to account for the converging beam and the different numbers of actuators. At this time it is unknown the extent to which having DM_2 in a converging beam will affect our ability to achieve the contrast target. This will be a significant part of our test and is acknowledged as a main risk in § 3.4.

3.3. Mask design and manufacture. The previous ripple mask optimized for the HCIT was 30mm large, and it was designed for a 32 by 32 DM (hence, the outer working angle for which the mask was designed was $32 \lambda/D$). For this series of tests we have chosen to design masks for two

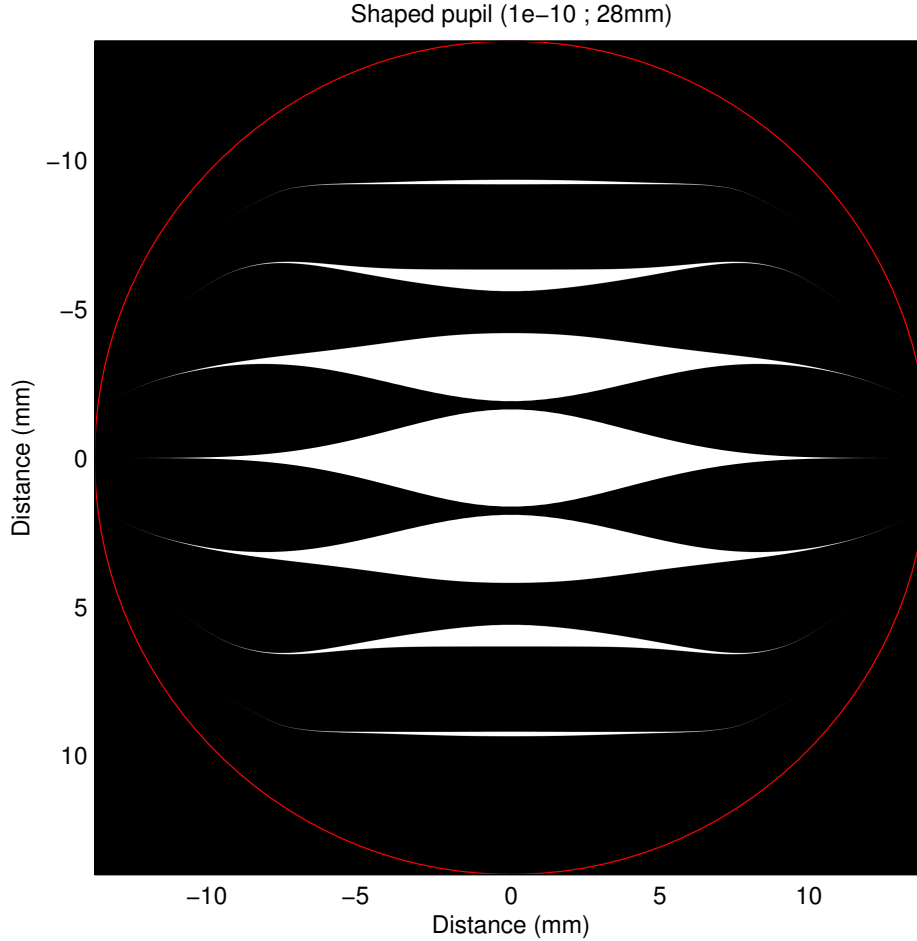


FIGURE 7. Transmission of the 10^{-10} , $56 \lambda/D$ mask. White areas are transmissive. The red circle illustrates the pupil diameter.

cases: in the first case 56 actuators of DM_1 are used, whereas 48 are used in the second case. This makes the OWA of the mask's point-spread functions 56 and $48 \lambda_{min}/D$, respectively (λ_{min} is the minimum wavelength when observing in broadband). It also makes the masks 28 and 24mm large, respectively. Figure 7 illustrates the transmission of the 10^{-10} , $56 \lambda/D$ mask.

In addition, we wanted the new ripple masks to create either a 10^{-10} contrast or a 10^{-7} contrast. The 10^{-10} contrast mask is specifically designed to satisfy the goals of the project milestone. We hope to demonstrate with the 10^{-7} contrast mask that stroke minimization can be used to create high-contrast below the nominal contrast of the coronagraph.

Four different ripple masks are thus being manufactured for the HCIT, using deep reactive ion etching (DRIE). Similar masks have also been designed for Princeton HCIL so that comparisons could be made (these are 10mm wide), though due to scheduling problems those tests will have to be done concurrently rather than prior to our HCIT run as proposed. As was the case in 2007, when shaped pupils were used in the HCIT for the first time, features too small to make with the etching process have been converted to dashes (see ? and Fig. 8).

Focal plane masks (FPM) have been designed for these masks (one for the HCIT, and one for the HCIL). Contrary to masks manufactured in 2007, the usually sharp corners of the masks have been rounded to reduce diffraction effects. FPM's have been designed for monochromatic (808nm

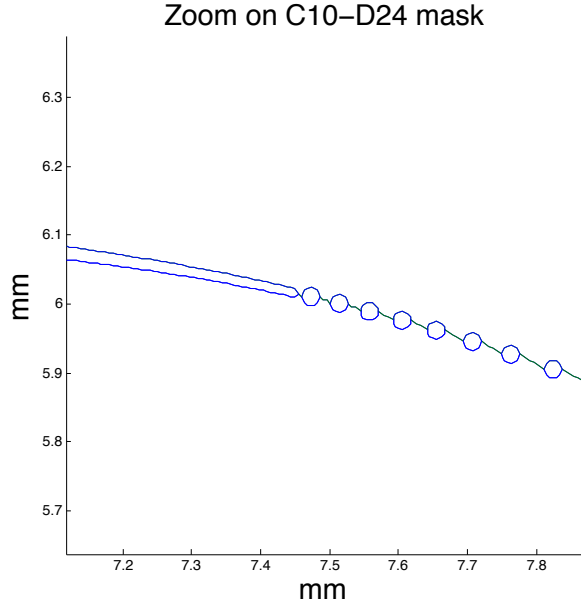


FIGURE 8. A zoomed in image of the design of thin end of one of the mask openings. Note that as the opening becomes smaller than a minimum feature size it is replaced by a sequence of fixed diameter “dashes” with the same total transmission. This avoids complex electric field guiding effects through narrow openings with high side-walls.

in the HCIT, 635nm in the HCIL) and broadband (760-840nm in the HCIT, 550-705nm in the HCIL) operation modes.

Figure 9 shows the location of the masks on a first wafer. Two lower-priority masks could not be placed on that first wafer (the 10^{-7} , $48\lambda/D$ mask for the HCIT and the focal plane mask for the HCIL). The two remaining masks will most likely be part of a second wafer. Spares of the top-priority masks will also be placed on the second wafer (the 10^{-10} , 56 and $48\lambda/D$ mask for the HCIT).

3.4. Experiment Risks. As noted above, since this is a new configuration for the HCIT and the first time very high contrast experiments have been done with two deformable mirrors, there are several identifiable risks that, if realized, could affect our ability to achieve the milestones or, at the least, degrade the contrast achieved. In this section we list the main risks and discuss our approach to minimizing them.

Hardware Risks:

- Alignment and registration procedures of the DMs. Before running an experiment at Princeton’s HCIL, we center both DMs on the shaped pupil and clock them to match the orientation of the shaped pupil mask. At the HCIT, the DMs are aligned at the beginning of all tests, and any drifts or rotations afterwards are just measured and accounted for in the optical model. We will need to include these translational and rotational shifts of the DMs and shaped pupil in our control and estimation algorithms. The HCIT has experience using phase diversity to determine the actuator gains of and surface map of DM1, which is at a pupil, but has not yet attempted to use the same process for determining the actuator gains and surface map of DM2, which is located in the converging beam. Our controller

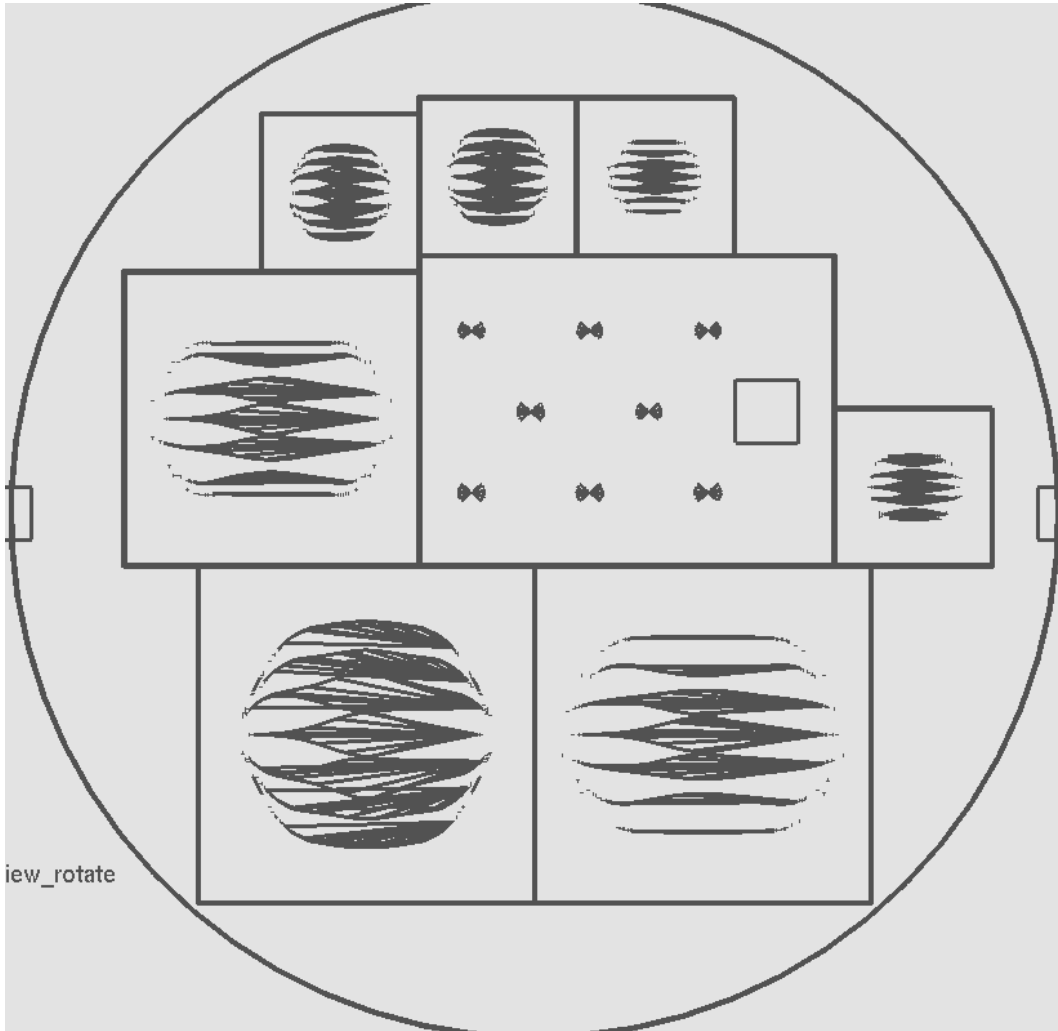


FIGURE 9. Schematic of the first wafer. Courtesy of Victor E. White.

and estimator are based on a model of the DMs, so adequate characterization of DM2 is necessary to achieve high contrast.

- Mask manufacture failure. The new configuration of the HCIT includes new DMs of different size and pitch than our tests in 2007. This new pupil size required us to manufacture new shaped pupils, as described in § 3.3. It took several months before the new configuration of the HCIT was defined and understood, leaving a shorter period than we had hoped for making the new masks. These masks are in manufacture and should be delivered on time. However, there is always a risk in this delicate process that the masks may fracture, etch unevenly, or otherwise not meet requirements. This would likely cause us to miss our scheduled HCIT run and cause significant delays.
- New etching process. In an effort to reduce the affects of large sidewalls on the shaped pupil performance, the JPL Microdevices Laboratory is using new, thinner wafers and experimenting with a new etching process. The nominal mask thickness is $40\ \mu\text{m}$, only $10\ \mu\text{m}$ thinner than our previous masks. The thin mask is $10\ \mu\text{m}$, a significant departure. Since both are new, there is some risk that they will not work, though the risk is smaller for the $40\ \mu\text{m}$ mask.

- Converging beam. As mentioned earlier, a significant departure in the HCIT configuration from that at Princeton is the location of DM2 in a converging beam. In order to minimize the time and expense required to reconfigure for 2 DMs, the second DM is replacing an existing flat. Consequently, it is located in a converging beam. This requires a modification to the correction algorithms, which is in process, and could have unpredicted consequences on the ability to achieve the dark holes desired. Analysis and simulation are in process.

Schedule Risks:

- Vacuum recycling due to alignment challenges. The current schedule assumes that all optics are aligned and tested, the chamber is pumped down, and testing begins. However, since the HCIT has never been operated with 2 DMs, there is some risk that the alignment and registration between the DMs will be more challenging than expected and several pump down cycles will be required. This has a significant impact on the test schedule.
- Software compatibility. All of the algorithms for estimation and control at Princeton need to be interfaced with the HCIT control software. There is a small risk of problems here.
- Replacing DM1 aperture mask. Our current plan is to perform two tests, one with a smaller pupil stop on DM1 exposing only a 48-actuator diameter circle and one with a larger pupil stop exposing a 62-actuator diameter circle. The latter mask allows a broader range of control but exposes actuators not used before. Bad actuators or a rough surface- mostly located outside the inner 56×56 -actuator region - could result in stray light not blocked by the shaped pupil. There is some schedule risk in changing the aperture stops because the vacuum must be cycled in order to install a different pupil stop in front of DM1.

There are several actions that can mitigate this risk. First among them is to have as much information as possible about the HCIT layout and, in particular, the properties of DM2. The first week of testing is planned to be spent characterizing the newly installed DM2. A significant effort will also be spent during the room temperature testing to ensure full software compatibility between Princeton’s HCIL and JPL’s HCIT. Finally, should the characterization plans for DM2 fail, we have a backup method using an analytical approach for modeling DM2.

4. CONTRAST MEASUREMENT AND DATA ANALYSIS

In this section we describe the process of calibrating the system and taking the final contrast measurements for the milestone. We also include a discussion of how the data is analyzed to develop the confidence limits need to satisfy the milestone. We begin with a set of definitions common to other TDEM whitepapers describing experiments in the HCIT.

4.1. Definitions. Our milestone is defined as the contrast achieved in a dark hole close to the central PSF of the simulated star. Establishing the milestone requires a measurement of the intensity of the speckles appearing within the dark field and calibrating relative to the intensity of the incident star. The measured contrast will be assessed in terms of statistical confidence to capture the impact of experimental noise and uncertainties. In the following paragraphs we define the terms involved in this process, spell out the measurement steps, and specify the data products.

- (1) “Raw” Image and “Calibrated” Image. Standard techniques for the acquisition of CCD images are used. We define a *raw image* to be the pixel-by-pixel image obtained by reading the charge from each pixel of the CCD, amplifying and sending it to an analog-to-digital converter. We define a *calibrated image* to be a raw image that has had background bias subtracted. Saturated images are avoided in order to avoid the confusion of CCD blooming and other potential CCD nonlinearities. All raw images are permanently archived and available for later analysis.
- (2) We define “scratch” to be a DM setting in which actuators are set to a predetermined surface figure that is approximately flat.

- (3) We define the “star” to be a small pinhole illuminated with monochromatic, narrow band, or broadband light relayed via optical fiber from a source outside the HCIT vacuum wall (e.g., the supercontinuum white light source or monochromatic laser). Here, by “small” we mean that it is to be unresolved by the optical system. This “star” is the only source of light in the optical path of the HCIT. It is a stand-in for the star image that would have been formed by a telescope system.
- (4) We define the “algorithm” to be the computer code that takes as input the measured speckle field image, and produces as output a voltage value to be applied to each element of the DM, with the goal of reducing the intensity of speckles.
- (5) The “contrast field” is a dimensionless map representing, for each pixel of the detector, the ratio of its value to the value of the peak of the central PSF that would be measured in the same testbed conditions (light source, exposure time, Lyot stop, etc.) if the coronagraph focal plane mask were removed. The calibration of the contrast field is further detailed in Section 4.2.
- (6) The “dark hole” is the region in the image plane where the desired controlled high-contrast is achieved. It is bound by the “inner working angle” and “outer working angle”.
- (7) The “contrast value” is a dimensionless quantity that is the average value of the contrast field over the dark hole adopted for the experiment.
- (8) “Statistical Confidence”. The interpretation of measured numerical contrast values shall take into consideration, in an appropriate way, the statistics of the measurement, including detector read noise, photon counting noise, and dark noise.

4.2. Measurement of the Star Brightness. In order to calibrate the final measurements of the contrast field into units of contrast, a measurement of the brightness of the artificial star is needed. From reading previous reports, we found this has been done two ways. The first measured the star brightness at the full intensity used for the experiment at very short integration times (averaging over many exposures to reduce photon and read noise). This provided an exposure time calibration (that is, an intensity of the star in average counts/sec). The long exposure images of the contrast field were then calibrated by dividing dark hole counts by the exposure time calibration multiplied by the actual exposure time. There are two potential pitfalls with this method. First, the laser must be operated at a level for the entire experiment that allows the initial short exposure measurements (within the exposure time limits of the camera). Second, the exposure time scaling is assumed to be linear over many orders of magnitude (the short exposures can be milliseconds while the final dark hole exposures can be tens of seconds to minutes).

The second approach is to compare the star intensity with the focal plane mask removed to the intensity of a bright area of the PSF field not in the contrast field and not covered by the focal plane mask when it is in place. This provides a calibration of that field point contrast to the central star. Once the star is covered by the focal plane mask, that field point is used to provide the contrast for the dark hole. This is the approach to be used for the milestone tests. The central star image without a focal-plane mask will be used to calibrate the quilting orders of DM2 at $\pm 23 \lambda/D$. When the focal-plane mask is put in place, the visible quilting orders are then used to calibrate the contrast in the dark hole. The main pitfall of this approach is the same as above—the laser must be operated at a fixed power that allows measurements of the star peak within the exposure time limits of the camera. This implies that the camera gain is constant over the range of exposure times and that the laser power is stable. Fortunately, measurements have shown the laser power to be sufficiently stable over the time scales of the experiment. Accuracy of the calibration also relies on the assumption that the calibration region of the field remains sufficiently unaltered over the course of the control iterations to remain an accurate source of calibration.

4.3. Measurement of the Coronagraph Contrast Field. After the process of wavefront control and estimation described in § 2 is completed, the average contrast within the contrast field is

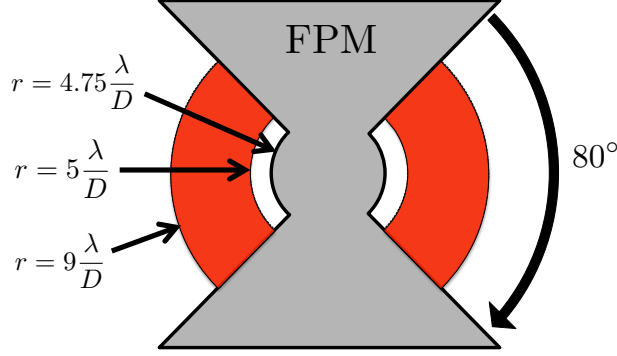


FIGURE 10. The symmetric dark holes, shown in red, are 80° segments (the maximum allowed by the focal plane mask) of a ring spanning a radius of 5 to $9 \lambda/D$. The focal plane mask (FPM), shown in gray, blocks a circle of radius $4.75 \lambda/D$.

measured for each experiment run. For both the primary milestone (monochromatic at 808 nm) and secondary milestone (10% band using 5 2% filters on a super continuum source), this average contrast is obtained as follows:

- (1) The occulting focal-plane mask is centered on the star image.
- (2) A long-exposure (tens-of-seconds) image is taken of the coronagraph contrast field. That field is defined by two 80° segments of a ring on either side of the star as shown in Fig.10. The arcs range from a radius of $5 \lambda/D$ to $9\lambda/D$ as stated in the milestone.
- (3) Each pixel measurement in the contrast field is divided by the peak value of the reference star intensity as determined by the calibration procedure described in § 4.2.
- (4) The pixels within the contrast field are averaged to obtain the average contrast for each of the N_e experiments.

4.4. Milestone Demonstration Procedure. The full milestone demonstration procedure is as follows:

- (1) The DM is set to scratch with a reset of the wavefront control software, including any prior field estimates or control values.
- (2) Wavefront estimation and control iterations are performed (as described in § 2) to iteratively converge to settings of the DM actuator driver voltages that give an acceptable high-contrast solution for the target high-contrast field or until the algorithm ceases to improve. This typically takes from one to several hours, starting from scratch, if no prior information is used.
- (3) For the monochromatic milestone, a single long-exposure image is taken (or several images are taken and averaged) of the coronagraph contrast field as described in § 4.3. These exposure times should be short compared to stability time scales of the HCIT (see § 4.5 below). Only a single image is taken to avoid confusing the capability of the wavefront control algorithm with long-term instabilities in the HCIT.
- (4) For the broadband milestone, five measurements through each of the 2% (16 nm) filters are taken to comprise the full bandpass from 760nm to 840 nm. The source is a supercontinuum laser.
- (5) All laboratory data are archived for future reference, including raw and calibrated images of the reference star and contrast field.
- (6) The experiment is repeated from scratch N_e times as cost and schedule allow.

4.5. Milestone Contrast Measurement and Confidence Limit. In this section we discuss the specific measurement model and how that leads to a contrast measurement. We then study the

statistics of that measurement to come to a confidence interval criteria for the milestone success. The measurement model and subsequent analysis follows closely the approach in ?.

We start by defining an intensity, I_{ij} , at pixel $\{i, j\}$ of the final image plane detector in terms of system characteristics including the coronagraph, wavefront aberrations, and DMs,

$$(11) \quad I_{ij} = \epsilon\eta\Delta\lambda [I_s(\lambda_r)P(0,0)\bar{P}_{ij} + b_{ij}] \Delta\alpha$$

where I_s is the artificial star irradiance in photo-electrons $\text{sec}^{-1} \text{m}^{-2} \mu\text{m}^{-1}$ at reference wavelength λ_r (the calibration of which is described in § 4.2), η is the overall throughput of the optical system, ϵ is the quantum efficiency, $\Delta\lambda$ is the observing waveband, $\Delta\alpha$ is the area of a single pixel in physical units (m), and b_{ij} is the irradiance of the incoherent background. The normalized point spread function of the system including coronagraph at each pixel is given by,

$$(12) \quad \bar{P}_{ij} = \frac{1}{\Delta\alpha} \int \int_{\Delta\alpha_{ij}} \bar{P}(\lambda_r, u, v) dudv.$$

where \bar{P} is the normalized continuous point spread function, $\bar{P} = P(u, v)/P(0, 0)$, and $P(u, v)$ is the continuous PSF of the system including aberrations and control.¹ The expression for the PSF in terms of system parameters is described in ?. Note that the goal of the combined coronagraph and wavefront control is to reduce the value of the PSF in the dark hole to below the contrast requirements. We are only interested, then, in the values of \bar{P}_{ij} for indexes within the dark hole.

The actual photon arrival rate at each pixel is given by a Poisson process. If we let Z_{ij} equal a random variable equal to the photon count at detector pixel i, j in time t , then the probability that it equals a particular measured value z_{ij} is given by

$$(13) \quad \Pr[Z_{ij} = z_{ij}(t)] = e^{-I_{ij}t} \frac{(I_{ij}t)^{z_{ij}}}{z_{ij}!}.$$

As usual, the mean and variance of Z_{ij} are given by

$$(14) \quad \mathcal{E}[Z_{ij}] = I_{ij}t = \mu_{ij}(t)$$

$$(15) \quad \mathcal{E}\left\{[Z_{ij} - \mu_{ij}(t)]^2\right\} = I_{ij}t = \sigma_{ij}^2(t)$$

where $\mathcal{E}\{\cdot\}$ is the expected value operator. We can simplify the analysis by assuming a large enough integration time t such that the Poisson arrival statistics are well approximated by a normal distribution. This lets us write the measured photon count at each pixel as a simple linear model consisting of the mean arrival plus a zero mean additive Gaussian random variable([?]),

$$(16) \quad z_{ij} = C_s\bar{P}_{ij} + C_s\bar{b}_{ij} + \nu_{ij}$$

where $C_s\bar{P}_{ij}$ is the mean photon count, $\mu_{ij}(t)$, from the star, C_s is the artificial star intensity scale factor, and \bar{b}_{ij} is the normalized mean photon count from the incoherent background. The noise term, ν , is a zero mean, Gaussian random variable representing the photon statistics and read noise. Its variance is given by $\sigma_\nu^2 = C_s\bar{P}_{ij} + C_s\bar{b}_{ij} + \sigma_r^2$.

To put the photon count measurement at each pixel into units of contrast, we divide by the peak value of the PSF, C_s , which is obtained by the calibration procedure described in § 4.2. Denoting the measurements in units of contrast by \bar{z}_{ij} , the contrast measurement is given by

$$(17) \quad \bar{z}_{ij} = \bar{P}_{ij} + \bar{b}_{ij} + \bar{\nu}_{ij}$$

where $\bar{\nu}_{ij}$ is the normalized noise term with variance $\sigma_\nu^2 = \frac{\bar{P}_{ij} + \bar{b}_{ij}}{C_s} + \sigma_r^2/C_s^2$. In units of contrast, the standard deviation of the noise is a signal-to-noise metric. The photon noise component gets smaller as $1/\sqrt{t}$, the read noise component stays constant.

¹For apodized coronagraphs such as we are testing here, this is a well defined definition of contrast. For systems with image plane masks such as Bandlimited Lyot and Vortex the nominal PSF is zero in a perfect system. Here, the normalization is by the central value of the PSF without the image plane mask (but with the Lyot stop).

Eq. 17 represents the measurements at a pixel for every image, those in the control iterations as well as the final milestone measurements. The control and estimation process described in § 2.2 and § 2.3 involves many images over minutes to hours to converge to a final contrast. While the statistics of those images and the behavior of the algorithms is interesting and important, particularly for diagnosing performance problems, they are not relevant to the final contrast milestone. The milestone metric only asks for the contrast after the final step of the control algorithm. What did the combined coronagraph and wavefront control system accomplish and is it good enough for science? The final step is defined as either when the milestone is met or when the contrast ceases to change by a specified amount, leading to a declaration of convergence. Thus, for the purposes here, Eq. 17 will be taken to represent the contrast measurement per pixel for a given integration time t in the final image after convergence of the control algorithms in each of the experiment runs.

There are four sources of randomness in Eq. 17 that will affect establishing confidence intervals on the final contrast metric. The first is the possible variation in the speckle background, given by the values of \bar{P}_{ij} in the dark hole. It is well known that the wavefront can vary over time due to temperature fluctuations, vibration, misalignments and drift, and other sources of error. This causes the speckles to change intensity across the dark hole over some time-scale. (An excellent reference on the probabilistic modeling of speckle motion is that by ?.) In other words, \bar{P}_{ij} is itself a random variable. Fortunately, these changes should be slow compared to an integration time in the HCIT. Understanding and controlling them is certainly important to ensure the effectiveness of the wavefront control algorithm, since the total time for all iterations to converge can be very long. In fact, the speckle variation is one source of the fundamental contrast floor achievable. However, this should play a small role in the confidence limits of a single image measurement of contrast (Eq. 17). Nevertheless, it is one of the sources of variations across the experimental set of final contrast measurements.

The second random variable is the incoherent background, \bar{b}_{ij} . It is speculated that there is a background light level in the HCIT uncorrectable by the DMs. It is impossible to generate a raw contrast below that level. It is likely that this incoherent background also varies randomly with time, adding a source of randomness to Eq. 17. However, it is highly unlikely that variation will be fast on the timescale of the single image integration time. We thus consider \bar{b}_{ij} to be a constant over the integration time.²

The third source of randomness in the final contrast measurement given by Eq. 17 is photon noise, represented by ν_{ij} . The photon noise is kept small through choice of integration time. That is, we choose an integration time such that $\frac{1}{\sqrt{C_s \bar{P}_{ij} + C_s \bar{b}_{ij}}}$ is as small as practical compared to the other sources of randomness.

The fourth and final source of randomness is the variation in experimental conditions from one run of the controller to another. A single experiment, starting from scratch, that achieves a certain average contrast (defined below), doesn't demonstrate that the process is repeatable. We would like to gain confidence that every run, from arbitrary initial conditions, will reach the desired contrast level. In other words, there exists a set, or ensemble, of all possible outcomes of HCIT experiments starting from scratch. The variations across this set come from a variety of factors, including small changes in initial conditions due to drifts and thermal changes, noises in the system, environmental conditions and other factors. While it would be laudable to try and fully characterize this set and to extrapolate to a space mission, that is unrealistic. The best we can do in these TDEM

²Note that speckle variation with time and incoherent background are only two of the possible sources limiting the ultimate contrast achieved. Other systematic errors include limitations of the estimation and control algorithms, physical limitations of what wavefront can be achieved via summing influence functions on a DM, errors in the DM surface model and failed actuators. In addition, if the integration time of the images in each iteration is not sufficiently long, photon noise can limit the contrast achievable by the algorithm.

experiments is perform a small number of experiments and confirm, with some confidence, the achievable contrast in some subset of the ensemble.

Since we don't know *a priori* the variance in contrast due to these sources of error, the only approach available to defining confidence intervals and thus assure some level of confidence in our milestone claim is to estimate the statistics from the data. We describe this next.

We start by modifying Eq. 17 slightly by adding a superscript k to index each experimental run,

$$(18) \quad \bar{z}_{ij}^k = \bar{P}_{ij}^k + \bar{b}_{ij}^k + \nu_{ij}^k \quad k = 1 \dots N_e$$

where N_e is the number of independent experiments. The average contrast for the milestone metric is defined over a set \mathcal{H} of n_p pixels that we call the dark hole. We thus find the average contrast for experiment k by summing over all pixels,

$$(19) \quad c^k = \frac{1}{n_p} \sum_{\{i,j\} \in \mathcal{H}} \bar{z}_{ij}^k = \frac{1}{n_p} \sum_{\{i,j\} \in \mathcal{H}} \bar{P}_{ij}^k + \bar{b}_{ij}^k + \nu_{ij}^k \quad k = 1 \dots N_e.$$

The milestone is defined by the *expected* average contrast, $\mu_c = \mathcal{E}\{c^k\}$, and the expected variance, $\sigma_c^2 = \mathcal{E}\{(c^k - \mu_c)^2\}$ (coming from the combination of speckle statistics, photon noise, and experimental variation). In other words, based on our measurements we would like to know that

$$(20) \quad \mu_c + 3\sigma_c \leq c$$

with 90% confidence, where c is the defined contrast limit in the milestone statement for either monochromatic or broadband light. Since we can't, of course, run all possible experiments in the ensemble to find μ_c and σ_c , we estimate the expected value by taking the sample mean of the N_e experiments run,

$$(21) \quad \hat{c} = \frac{1}{N_e} \sum_{k=1}^{N_e} c^k.$$

The sample variance is then given by the usual formula,

$$(22) \quad \hat{s}_c^2 = \frac{1}{N_e - 1} \sum_{k=1}^{N_e} (c^k - \hat{c})^2.$$

For simplicity, and absent any other information, we assume that c^k is normally distributed (with mean μ_c and standard deviation σ_c).³ Since we don't know the underlying mean and variance, we must use our sample mean and variance in our evaluation of the milestone. However, since these too are random variables, we must account for the standard deviation of each as well to be conservative. The confidence interval on the estimate of the mean, \hat{c} , assuming a small sample size is given by the Student t -statistic with $N_e - 1$ degrees of freedom,

$$(23) \quad \mu_c = \hat{c} \pm t_{\alpha_1/2} \frac{\hat{s}_c}{\sqrt{N_e}}$$

where the confidence level is given by $1 - \alpha_1$. That is, since we are only interested in the upper bound, $\Pr[\mu_c < \hat{c} + t_{\alpha_1/2} \frac{\hat{s}_c}{\sqrt{N_e}}] = 1 - \alpha_1$.

Likewise, the confidence intervals for the estimate of the variance are given by the χ^2 statistic with $N_e - 1$ degrees of freedom,

$$(24) \quad \frac{(N_e - 1)\hat{s}_c^2}{\chi_{\alpha_2/2}^2} \leq \sigma_c^2 \leq \frac{(N_e - 1)\hat{s}_c^2}{\chi_{1-\alpha_2/2}^2}.$$

³This is probably a good assumption, at least with regards to the speckle statistic and photon noise, as each estimate comes from summing over many pixels, allowing us to use the central limit theorem to argue that the distribution is Gaussian.

The final test metric for the milestone uses the upper bounds on each confidence interval to become

$$(25) \quad \hat{c} + t_{\alpha_1/2} \frac{\hat{s}_c}{\sqrt{N_e}} + 3 \sqrt{\frac{(N_e - 1)}{\chi_{1-\alpha_2/2}^2}} \hat{s}_c \leq c.$$

What remains is to find the values of α_1 and α_2 to get our desired 90% confidence in the test. In the final analysis we will choose a variety of values looking for the best balance between the confidence in the mean and the confidence in the standard deviation. Here, absent any knowledge of the outcomes, the sensible choice is to split evenly between the two. That is, we set $\Pr[\mu_c < \hat{c} + t_{\alpha_1/2} \frac{\hat{s}_c}{\sqrt{N_e}}]$ and $\Pr[\sigma_c^2 < \frac{(N_e - 1)\hat{s}_c^2}{\chi_{1-\alpha_2/2}^2}]$. Assuming the two probabilities are independent, the total probability is just the product of the two, leaving

$$(26) \quad (1 - \alpha_1)(1 - \alpha_2) = 0.9.$$

Assuming equal confidence in both means we choose each of α_1 and α_2 such that the confidence interval is equal to $\sqrt{0.9} = 0.95$ for each. This completes the definition of our metric and establishes the success criteria for each milestone (Eq. 25).

It is worth noting again that success on the milestone isn't necessarily directly translatable to a space mission. Success here only states that the coronagraph and wavefront control system can correct for all the expected initial conditions within the HCIT (and the expected variation with time). A spacecraft is likely to be much less stable and one must extrapolate with care.

5. SUCCESS CRITERIA

The success of the experiment is measured by achieving the primary and secondary milestones in a reasonable number of experiments with repeatable experimental conditions. This demonstrates the basic feasibility of using two deformable mirrors in series to achieve high contrast dark holes on both sides of the image plane, both monochromatically and in 10% bands. We do not claim that this validates a particular design or approach that can be moved quickly to space nor do we make claims regarding how the results within the controlled HCIT environment might be extrapolated to a space mission. The success criteria can then be described as follows:

Primary Milestone:

- (1) Initialize the HCIT at vacuum and complete all alignments using one of the monochromatic lasers (or the broadband source with a 2% filter).
- (2) Calibrate the high-contrast coronagraph field as described in § 4.2.
- (3) Perform the wavefront estimation and control process and take contrast measurements in the high-contrast dark hole as described in § 4.4.
- (4) Compute the mean contrast over the dark hole as described in § 4.3.
- (5) Repeat the experiment from scratch N_e times.
- (6) Using the analysis procedure described in § 4.5, verify success by calculating the milestone success metric given in Eq. 25 for the monochromatic contrast requirement of 1×10^{-9} .

Secondary Milestone:

- (1) Initialize the HCIT at vacuum and complete all alignments using one of the monochromatic lasers (or the broadband source with a 2% filter).
- (2) Switch to the broadband supercontinuum source and dial in the appropriate 2% filters using the filter wheel. Calibrate the high-contrast coronagraph field as described in § 4.2.
- (3) Perform the wavefront estimation and control process and take contrast measurements in the high-contrast dark hole as described in § 4.4. For broadband, experiments will be

performed using a single narrow band measurement and wavelength extrapolation as well as sequential measurements in each of the five narrow bands.

- (4) Compute the mean contrast over the dark hole as described in § 4.3 by averaging the measurements in each of the five bands.
- (5) Repeat the experiment from scratch N_e times.
- (6) Using the analysis procedure described in § 4.5, verify success by calculating the milestone success metric given in Eq. 25 for the broadband contrast requirement of 5×10^{-9} .

6. CERTIFICATION & DATA SHARING

The PI will assemble a milestone certification data package for review by the ExEPTAC and the ExEP program. In the event of a consensus determination that the success criteria have been met, the project will submit the findings of the review board, together with the certification data package, to NASA HQ for official certification of milestone compliance. In the event of a disagreement between the ExEP project and the ExEPTAC, NASA HQ will determine whether to accept the data package and certify compliance or request additional work.

The milestone certification data package will contain the following explanations, charts, and data products.:

- (1) A narrative report, including a discussion of how each element of the milestone was met, and a narrative summary of the overall milestone achievement.
- (2) A complete description of the HCIT layout and optical system used with the significant characteristics
- (3) The sets of images used for calibration of the reference star.
- (4) Microscope images of the shaped pupil and focal plane masks with simulated PSFs.
- (5) Calibrated final images of the coronagraph contrast field for each experiment run, for both the monochromatic and broadband experiments.
- (6) Calibrated curves showing the contrast convergence of the control algorithm for all runs.
- (7) A histogram of the brightness distribution of pixels in the dark hole for each of the final images in the data set and for the combined data.

7. LIST OF ACRONYMS

AIC	Achromatic Interference Coronagraph
AO	Adaptive Optics
APLC	Apodized Lyot Coronagraph
APRA	Astrophysics Research and Analysis
CCD	Charge Coupled Device
DM	Deformable Mirror
DRIE	Deep Reactive Ion Etching
FPM	Focal Plane Mask
FPWS	Focal Plane Wavefront Sensing
HCIL	High-Contrast Imaging Laboratory
HCIT	High-Contrast Imaging Testbed
IWA	Inner Working Angle
JPL	Jet Propulsion Laboratory
NASA	National Aeronautics and Space Administration
NESSF	NASA Engineering and Space Science Fellowship
OAP	Off-axis Parabola
OWA	Outer Working Angle
PIAA	Phase Induced Amplitude Apodization
PSF	Point Spread Function
TDEM	Technology Development for Exoplanet Missions
TRL	Technology Readiness Level